Cyclization dynamics of finite-length collapsed self-avoiding polymers

Julian Kappler,[1] Frank Noé,[2] and R. R. Netz[1]
[1]*Dept. of Physics, Freie Universität Berlin, 14195 Berlin, Germany*
[2]*Dept. of Mathematics and Computer Science, Freie Universität Berlin, 14195 Berlin, Germany*
(Dated: February 22, 2018)

We study the end-point cyclization of ideal and interacting polymers as a function of chain length N. For the cyclization time τ_{cyc} of ideal chains we recover the known scaling $\tau_{\mathrm{cyc}} \sim N^2$ for different backbone models, for a self-avoiding slightly collapsed chain we obtain from Langevin simulations and scaling theory a modified scaling $\tau_{\mathrm{cyc}} \sim N^{5/3}$. By extracting the memory kernel $\Gamma(t)$ that governs the non-Markovian end-point kinetics, we demonstrate that the dynamics of a finite-length collapsed chain is dominated by the crossover between swollen and collapsed behavior.

The loop formation kinetics of polymers governs the dynamics of protein folding [1–3] and gene expression regulation[4–7] and consequently has been studied extensively both experimentally [1–3, 8, 9], and theoretically [4, 10–15]. The quantity of main interest is the cyclization time τ_{cyc}, i.e. the mean time it takes the two polymer ends to reach the cyclization radius R_{cyc} after starting from a distance $R_s > R_{\mathrm{cyc}}$. Pioneering theoretical works predicted τ_{cyc} for an ideal Gaussian chain to scale with the monomer number N as

$$\tau_{\mathrm{cyc}} \sim N^{\alpha} \tag{1}$$

with a crossover between $\alpha = 2$ for intermediate R_{cyc}, known as the Wilemski-Fixman (WF) scaling [10, 16], and $\alpha = 3/2$ for small R_{cyc}, known as the Szabo-Schulten-Schulten (SSS) scaling [14]. For interacting polymers the cyclization dynamics has been suggested, based on approximate analytical methods, to differ from the above scaling laws [17], only few numerical simulations of realistic chain models exist [18, 19]. For the particularly interesting case of a self-avoiding collapsed chain, as relevant for the initial steps of protein folding, very few results exist. Likewise, it is not clear whether realistic backbone models with constrained bond lengths and bond angles modify the cyclization dynamics.

In this paper we consider the end-to-end distance dynamics of three different polymer backbone models, namely the Gaussian (G), freely jointed (FJ), and freely rotating (FR) models, see Fig. 1 for illustrations. Furthermore we consider an interacting Gaussian chain that includes Lennard-Jones interactions (GLJ). From Langevin simulations we extract cyclization times τ_{cyc} and recover for non-interacting chains, depending on the cyclization radius R_{cyc}, the WF and SSS scaling laws, independent of the backbone model. However, for an interacting collapsed chain we find the asymptotic scaling $\tau_{\mathrm{cyc}} \sim N^{5/3}$, in agreement with scaling predictions for a collapsed chain [19]. Thus, cyclization dynamics is insensitive to polymer backbone details but substantially influenced by monomer-monomer interactions. To understand these results, we map the dynamics of the end-to-end distance R_{ete}, which is a collective variable that involves all polymer degrees of freedom [4, 11, 13], onto the generalized Langevin equation (GLE) that accounts for non-Markovian effects by a memory kernel $\Gamma(t)$ [17, 20–23]. We find that the memory kernels of ideal chains decay as $\Gamma \sim t^{-1/2}$ for intermediate times t irrespective of the backbone model, while for the interacting collapsed chain $\Gamma \sim t^{-6/11}$, which is the scaling of a swollen interacting chain. This demonstrates that the dynamics of a self-avoiding collapsed chain exhibits signatures of both collapsed and swollen chain behavior, which gives clues on the complex polymer relaxation kinetics observed in experiments [24–26].

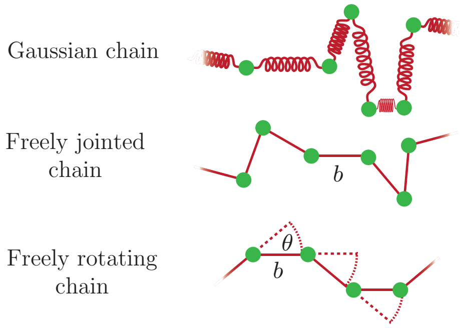

FIG. 1. Illustration of different backbone models considered. In the Gaussian model, neighboring monomers are bound by a harmonic potential. In the freely jointed model, the bond length b between neighboring monomers is constraint, in the freely rotating chain model both bond length b and bond angle θ are constraint.

We perform Langevin simulations at a temperature $T = 300$ K using the GROMACS 2016.3 simulation package [27] with parameters for alkane chains in implicit water from the gromos53a6 forcefield [28]. Friction coefficients approximate methane in water, while the masses are reduced by a factor of ten in order to minimize inertial effects, see the Supplemental Information (SI) [29] for details. Hydrodynamic interactions are neglected, which presumably are irrelevant for collapsed chain dynamics. For the Gaussian chain model neighboring monomers are subject to a harmonic potential which produces a mean distance of $b = 0.153$ nm. For the FJ model the distance between neighboring monomers is constrained to

$b = 0.153$ nm, in the FR model in addition the bond angles are constrained to $\theta = 111°$. All these models are ideal and monomers do not interact with each other. The GLJ model is based on the Gaussian chain model and includes the gromos53a6 Lennard-Jones (LJ) interactions for alkane chains [28], which produces a collapsed chain of self-avoiding segments that cannot cross each other [29].

We map our Langevin trajectories onto the GLE

$$\mu \ddot{R}_{\mathrm{ete}}(t) = -\int_0^t \mathrm{d}t' \, \Gamma(t-t') \dot{R}_{\mathrm{ete}}(t') - \nabla U(R_{\mathrm{ete}}(t)) + F_R(t), \tag{2}$$

where $R_{\mathrm{ete}} = \sqrt{(\vec{R}_{N-1} - \vec{R}_0)^2}$ is the scalar end-to-end distance, μ is an effective mass, ∇U is the derivative of the effective potential $U(R_{\mathrm{ete}})$, $\Gamma(t)$ is the memory kernel, and the random force $F_R(t)$ obeys the fluctuation-dissipation theorem (FDT) $\langle F_R(t) F_R(t') \rangle = k_{\mathrm{B}} T \, \Gamma(|t - t'|)$. All parameters of the GLE are extracted from the simulations, in particular, we calculate $\Gamma(t)$ using an extension of Berne's method [30] in the presence of a potential $U(R_{\mathrm{ete}})$ [31], see SI for details [29].

In Fig. 2 we compare memory kernels for the end-to-end distance vector, $\vec{R}_{\mathrm{ete}} = \vec{R}_{N-1} - \vec{R}_0$, of ideal Gaussian chains that are numerically extracted from simulations with analytical predictions based on the Mori-Zwanzig projection formalism [32, 33], see SI for details [29]. The agreement is perfect, which validates our numerical method for extracting $\Gamma(t)$ from simulation data. For $N \gtrsim 100$, $\Gamma(t)$ shows an intermediate $\Gamma \sim t^{-1/2}$ scaling regime, similar to recent results for the central monomer position of a Gaussian ideal chain [20, 22].

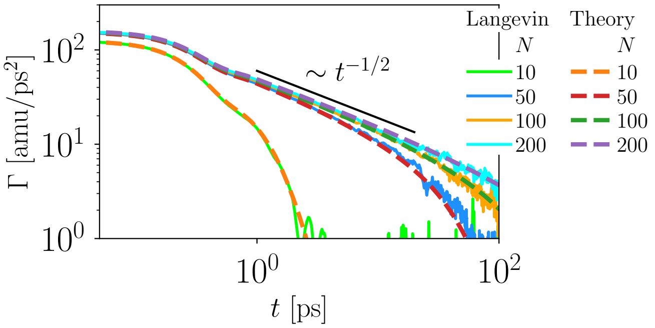

FIG. 2. Comparison of analytically and numerically calculated memory kernels for the end-to-end distance vector $\vec{R}_{\mathrm{ete}}$ of a Gaussian ideal chain.

Figure 3 (b) shows the potential U as a function of the end-to-end distance rescaled by the Kuhn length a_i, which is defined by $R^2_{\mathrm{ete}} \equiv a_i L$, where i = G, FJ, FR, GLJ indicates the respective chain model and L is the length of the fully extended chain, $L = (N - 1)b$. The potentals of the ideal chains are very similar while the results for the GLJ chain differ. This is reflected by the mean squared end-to-end distance R^2_{ete} in Fig. 3 (c), where all ideal chains yield a linear scaling $R^2_{\mathrm{ete}} = a_i b(N-1)$ with $a_{\mathrm{G}} = a_{\mathrm{FJ}} = b$, $a_{\mathrm{FR}} = b\sqrt{(1+\cos\theta)/(1-\cos\theta)}$ [34], which is consistent with the power-law scaling

$$R^2_{\mathrm{ete}} \sim N^{2\nu_{\mathrm{eq}}} \tag{3}$$

with the ideal-chain exponent $\nu_{\mathrm{eq}} = 1/2$. For the GLJ chain we observe swollen behavior for $N \lesssim 30$ with an exponent $\nu_{\mathrm{eq}} > 1/2$ [34] and a broad crossover to collapsed behavior for $N \gtrsim 100$ with an exponent $\nu_{\mathrm{eq}} = 1/3$ [35], as indicated by a broken line. This is expected, since our LJ parameters model a hydrophobic chain in water.

In Fig. 3 (d) we show simulation results for the mean squared displacement (MSDs) of R_{ete}, which for intermediate time display power laws according to

$$\Delta R^2_{\mathrm{ete}}(t) = \langle (R_{\mathrm{ete}}(t) - R_{\mathrm{ete}}(0))^2 \rangle \sim t^{\beta}. \tag{4}$$

From the size scaling of a diffusing subchain consisting of N_{sub} monomers, $R_{\mathrm{sub}} \sim N_{\mathrm{sub}}^{\nu_{\mathrm{dyn}}}$, the diffusion law for the MSD of the subchain position, $R^2_{\mathrm{sub}} \sim D_{\mathrm{sub}} t$, and the diffusivity of a freely draining chain, $D_{\mathrm{sub}} \sim 1/N_{\mathrm{sub}}$, one obtains $N_{\mathrm{sub}}^{2\nu_{\mathrm{dyn}}+1} \sim t$ and thus [34, 36–38]

$$\beta = 2\nu_{\mathrm{dyn}}/(1 + 2\nu_{\mathrm{dyn}}). \tag{5}$$

Here, the exponent ν_{dyn} characterizes the dynamic chain size and only in the asymptotic long-time large-polymer length limit equals the static exponent ν_{st}, as we will detail further below. For ideal chains with $\nu_{\mathrm{dyn}} = 1/2$ one obtains $\beta = 1/2$, which agrees well with simulations results for Gaussian and FJ chains in Fig. 3 (d), while for the FR chain model no clear power law is observed, see SI for a possible explanation [29]. For the GLJ chain, the simulation results are consistent with an exponent $\beta = 6/11$ slightly larger than 1/2 over two decades in time [36, 37], which follows from Eq. (5) for the exponent of a swollen chain $\nu_{\mathrm{dyn}} = 3/5$ [34], but not for the collapsed exponent $\nu_{\mathrm{dyn}} = 1/3$ which would yield $\beta = 2/3$ (clearly inconsistent with the simulation data). We thus observe swollen scaling $\nu_{\mathrm{dyn}} = 3/5$ for the MSD in Fig. 3 (d), while the equilibrium end-to-end distance in Fig. 3 (c) is characterized by collapsed scaling $\nu_{\mathrm{eq}} = 1/3$. This can be rationalized by the fact that the internal mean monomer distance $\langle (\vec{R}_0 - \vec{R}_i)^2 \rangle$ in Fig. 3 (e) indeed exhibits swollen scaling with $\nu > 1/2$ over spatial scales for which the MSD in Fig. 3 (d) is characterized by the swollen exponent $\beta = 6/11$.

To corroborate that the end-to-end distance dynamics is characterized by swollen chain statistics, we in Fig. 3 (f) show memory kernels extracted from Langevin simulations for $N = 200$. The kernel of the Gaussian chain scales as $\Gamma \sim t^{-1/2}$ and, except for short times, agrees quantitatively with the FJ chain, demonstrating that the end-to-end dynamics is insensitive to details of the backbone model. This power law, which we also find for the

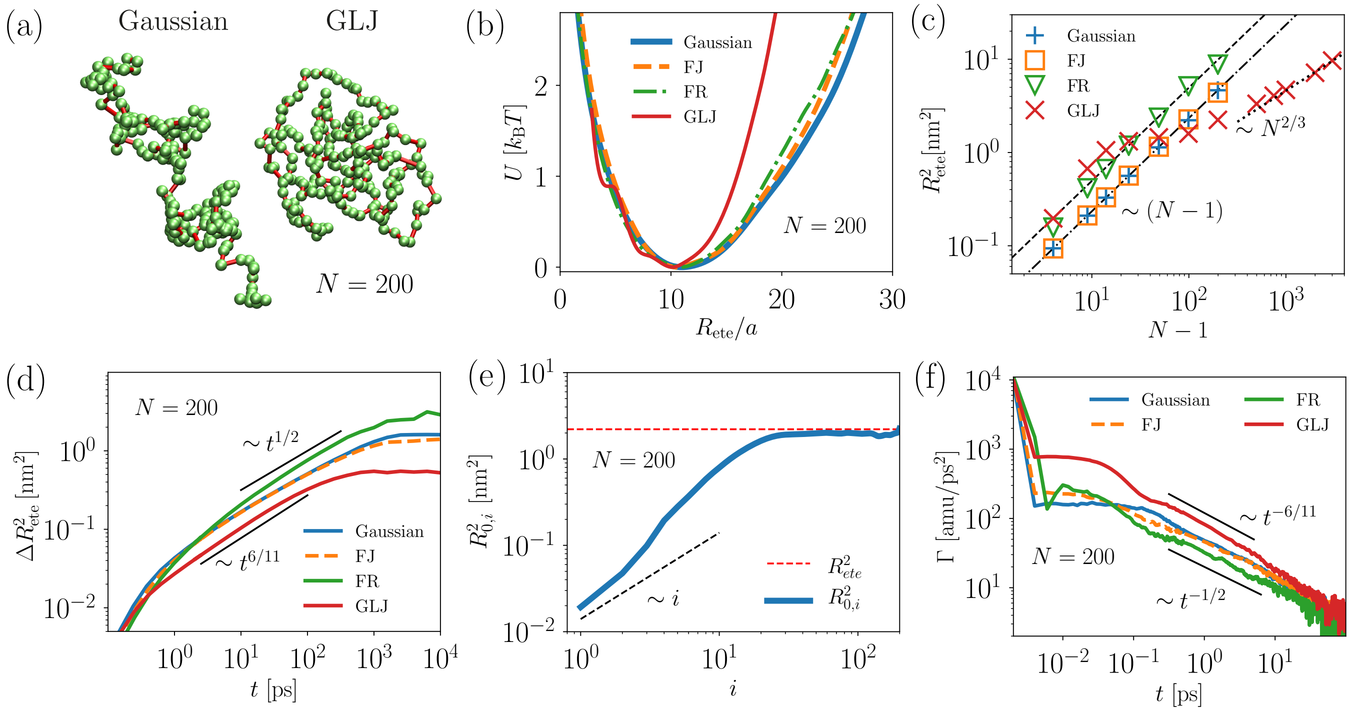

FIG. 3. (a) Simulation snapshots of Gaussian and GLJ chains. (b) Effective potential U for the end-to-end distance R_{ete} for $N = 200$. (c) Mean squared end-to-end distance as function of chain length N. Dashed and dashed-dotted lines show predictions for FR and G/FJ chain models, respectively. The dotted line indicates the power law $R^2_{\mathrm{ete}} \sim N^{2/3}$. (d) Mean-square displacement of the end-to-end distance. (e) Mean squared distance $R^2_{0,i} = (\vec{R}_0 - \vec{R}_i)^2$ between the terminal monomer and the i-th monomer of a GLJ chain. The red dashed line represents the mean end-to-end distance R^2_{ete}. (f) Memory kernels for chain length $N = 200$.

vectorial end-to-end separation $\vec{R}_{\mathrm{ete}}$ in Fig. 2, reflects the Rouse spectrum [20, 22]. Interestingly, Markov State Models for the polymer dynamics show similar power-law distribution of time scales, see SI [29]. The kernel of the FR chain model also scales as $\Gamma \sim t^{-1/2}$ with a prefactor that results from the different Kuhn length, as detailed in the SI [29]. The memory kernel of the interacting GLJ polymer model exhibits a different power law, consistent with $\Gamma \sim t^{-6/11}$, in agreement with the expected inverse relationship $\Delta R^2_{\mathrm{ete}}(t) \sim 1/\Gamma(t)$ [39], which is derived in the SI [29]. We conclude that the dynamics of an interacting collapsed chain is at intermediate times, for which we can extract the memory kernel, indeed characteristic of a swollen chain.

The cyclization time τ_{cyc} is defined as the mean time for R_{ete} to reach the cyclization radius R_{cyc} for the first time, starting from some end-to-end distance R_s, see the inset in Fig. 4 (a) for an illustration. The figure shows $U(R_{\mathrm{ete}})$ and τ_{cyc} for the GLJ model as a function of R_s for fixed $R_{\mathrm{cyc}} = 3a_{\mathrm{G}} \approx 0.46$ nm, denoted as a black vertical dashed line. For R_s not too close to R_{cyc}, τ_{cyc} is rather independent of R_s, so the scaling of τ_{cyc} should not critically depend on R_s, for which we use the minimum of U, indicated as colored vertical dashed lines.

In Fig. 4 (b) it is seen that τ_{cyc} exhibits power-law scaling according to Eq.(1). For ideal chains and rather large $R_{\mathrm{cyc}} = 3a_{\mathrm{G}} \approx 0.46$ nm, we obtain the ideal WF scaling $\alpha = 2$ [16]. This corresponds to the scaling of the chain relaxation time τ_{rel} and can be derived by equating the MSD, $\Delta R^2_{\mathrm{ete}}(t) \sim t^{\beta}$, Eq. (4), with the end-to-end radius, $R^2_{\mathrm{ete}} \sim N^{2\nu_{\mathrm{eq}}}$, Eq. (3), leading to $\tau_{\mathrm{rel}} \sim N^{\lambda}$ with [19]

$$\lambda = 2\nu_{\mathrm{eq}}/\beta = \nu_{\mathrm{eq}}(2\nu_{\mathrm{dyn}}+1)/\nu_{\mathrm{dyn}}, \tag{6}$$

where we used Eq. (5). For $\nu_{\mathrm{eq}} = \nu_{\mathrm{dyn}} \equiv \nu$ this reduces to $\lambda = 2\nu + 1$ [40, 41]. For an ideal chain with $\nu = 1/2$, and assuming that the chain relaxation times and cyclization times scale alike, we obtain the WF scaling $\alpha = \lambda = 2$ [16], as indeed observed for the ideal chains in Fig. 4 (b).

For very small cyclization radius, $R_{\mathrm{cyc}} \ll R_{\mathrm{ete}}$, the cyclization time will eventually exceed the chain relaxation time and cyclization becomes Markovian, in which limit τ_{cyc} is to leading order proportional to the inverse equilibrium probability for the two chain ends to be at the same position, thus $\tau_{\mathrm{cyc}} \sim R^3_{\mathrm{ete}} \sim N^{3\nu_{\mathrm{eq}}}$ and

$$\alpha = 3\nu_{\mathrm{eq}}. \tag{7}$$

For an ideal chain, $\nu_{\mathrm{eq}} = 1/2$, we recover the SSS scaling $\tau_{\mathrm{cyc}} \sim N^{3/2}$ [14], which indeed describes the simulation

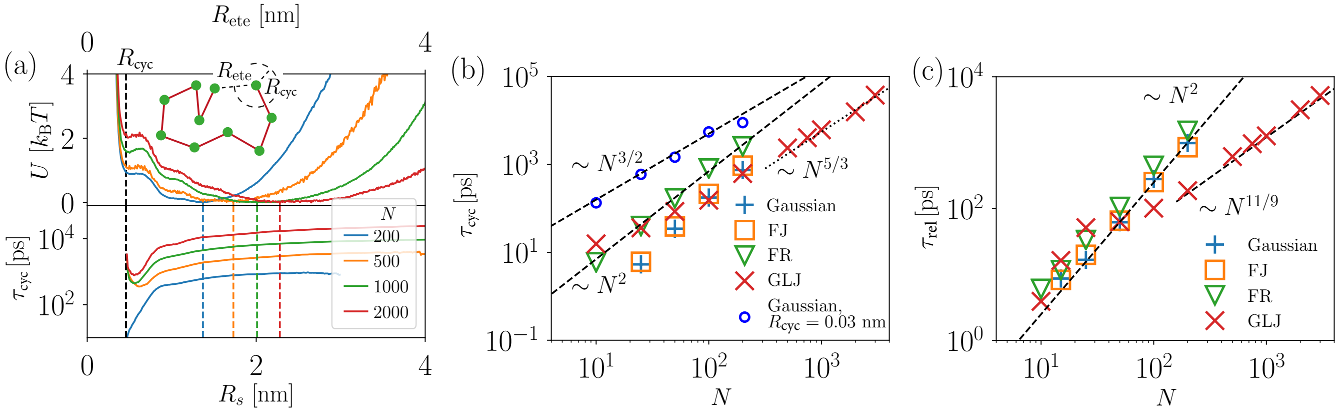

FIG. 4. (a) Effective potential U for the end-to-end distance of a GLJ chain as a function of $R_{\rm ete}$ (upper plot) and corresponding cyclization time $\tau_{\rm cyc}$ (lower plot) as a function of the starting position R_s. The cyclization distance $R_{\rm cyc} = 3a_{\rm G} \approx 0.46$ nm is denoted by a black vertical dashed line, each colored vertical dashed line denotes the respective position of the minimum of U. The inset illustrates the end-to-end distance $R_{\rm ete}$ and the cyclization radius $R_{\rm cyc}$. (b) Cyclization time as a function of chain length N, together with different scaling predictions indicated by lines. Except for the blue empty circles, where $R_{\rm cyc} = 0.03$ nm, the cyclization radius is $R_{\rm cyc} = 3a \approx 0.46$ nm. As starting position R_s the minimum of U is used. (c) Chain relaxation time $\tau_{\rm rel}$ as function of N. The definition of $\tau_{\rm rel}$ is illustrated in Fig. 5.

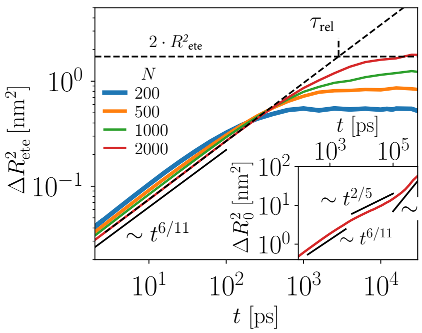

FIG. 5. The chain relaxation time $\tau_{\rm rel}$ is defined by the intersect of the short-time power-law behavior of the mean-square displacement of $R_{\rm ete}$ and the long-time limiting value. The dashed black lines illustrate this construction for $N = 2000$. The inset shows the MSD of a terminal monomer, $\Delta R_0^2(t) = \langle(\vec{R}_0(t) - \vec{R}_0(0))^2\rangle$, for $N = 2000$. The three different power-law scaling regimes are denoted by black bars.

data in Fig. 4 (b) for a small cyclization radius of $R_{\rm cyc} = 0.03$ nm $\approx a/15$.

For the collapsed chain data in Fig. 4 (b) we find a scaling exponent of $\alpha = 5/3$, which is in between the ideal limits of the SSS and WF scaling predictions and close to a recent analytical proposal [17]. While the SSS scaling for a collapsed chain with $\nu_{\rm eq} = 1/3$ predicts according to Eq. (7) $\alpha = 1$, the WF scaling for a collapsed chain with $\nu_{\rm eq} = \nu_{\rm dyn} \equiv 1/3$ correctly gives according to Eq.(6) $\alpha = \lambda = 5/3$, so that the observed scaling can be interpreted as a generalization of the WF scaling.

Curiously, for $\nu_{\rm dyn} = 1/3$ one would from Eq. (5) expect $\beta = 2/5$, in contrast to $\beta = 6/11$ (as follows from choosing $\nu_{\rm dyn} = 3/5$) seen in Figs. 3 (d) and 5. On the other hand, the scaling of the chain relaxation time in Fig. 4 (c) is rather consistent with the exponent $\lambda = 11/9$ which follows from Eq. (6) using $\nu_{\rm eq} = 1/3$ and $\nu_{\rm dyn} = 3/5$. The difference of the exponents α and λ characterizing the cyclization time $\tau_{\rm cyc}$ and the relaxation time $\tau_{\rm real}$ can be understood by considering the MSD of a terminal monomer of a $N = 2000$ GLJ chain, shown in the inset of Fig. 5, which exhibits three distinct scaling regimes: While for $t \lesssim 10^3$ ps the MSD displays swollen scaling, $\beta = 6/11$, for intermediate times 10^3 ps $\lesssim t \lesssim 10^5$ ps we observe collapsed scaling $\beta = 2/5$, until for longer times diffusive behavior $\beta = 1$ is found. We thus expect collapsed scaling to only become relevant on time scales $t \gtrsim 10^3$ ps, and indeed the cyclization times of the GLJ chains shown in Fig. 4 (b) are of that order. The corresponding relaxation times in Fig. 4 (c) on the other hand are of the order $\tau_{\rm MSD} \lesssim 10^3$ ps, and thus still dominated by swollen statistics, characterized by the exponent $\lambda = 11/9$.

In conclusion, the cyclization dynamics of a slightly collapsed, self-avoiding chain is characterized by a universal exponent $\alpha = 5/3$ which is in between the classical SSS and WF predictions of 3/2 and 2. Because a finite-length collapsed self-avoiding polymer exhibits a complex crossover of swollen to collapsed statistics, the scaling of cyclization time $\tau_{\rm cyc}$ differs for finite chain lengths from the scaling of the relaxation time $\tau_{\rm rel}$. Our comprehensive picture of the cyclization crossover dynamics applies to the dynamics of intra-chain distances as probed in the collapsed globular state of proteins [26, 42].

Funding by the DFG (Deutsche Forschungsgemeinschaft) via grant SFB 1114 / B02 is acknowledged.

---

[1] L. Milanesi, J. P. Waltho, C. A. Hunter, D. J. Shaw, G. S. Beddard, G. D. Reid, S. Dev, and M. Volk, Proceedings of the National Academy of Sciences **109**, 19563 (2012).

[2] L. J. Lapidus, W. A. Eaton, and J. Hofrichter, Proceedings of the National Academy of Sciences **97**, 7220 (2000).

[3] O. Bieri, J. Wirz, B. Hellrung, M. Schutkowski, M. Drewello, and T. Kiefhaber, Proceedings of the National Academy of Sciences **96**, 9597 (1999).

[4] A. Amitai and D. Holcman, Physics Reports **678**, 1 (2017).

[5] H. Krämer, M. Niemöller, M. Amouyal, B. Revet, B. von Wilcken-Bergmann, and B. Müller-Hill, The EMBO Journal **6**, 1481 (1987).

[6] S. Kadauke and G. A. Blobel, Biochimica et Biophysica Acta (BBA) - Gene Regulatory Mechanisms **1789**, 17 (2009).

[7] S. Holwerda and W. d. Laat, Frontiers in Genetics **3** (2012), 10.3389/fgene.2012.00217.

[8] L. J. Lapidus, P. J. Steinbach, W. A. Eaton, A. Szabo, and J. Hofrichter, The Journal of Physical Chemistry B **106**, 11628 (2002).

[9] H. Sahoo, D. Roccatano, M. Zacharias, and W. M. Nau, Journal of the American Chemical Society **128**, 8118 (2006).

[10] G. Wilemski and M. Fixman, The Journal of Chemical Physics **58**, 4009 (1973).

[11] T. Guérin, O. Bénichou, and R. Voituriez, The Journal of Chemical Physics **138**, 094908 (2013).

[12] D. J. Bicout and A. Szabo, The Journal of Chemical Physics **106**, 10292 (1997).

[13] T. Guérin, O. Bénichou, and R. Voituriez, Nature Chemistry **4**, 568 (2012).

[14] A. Szabo, K. Schulten, and Z. Schulten, The Journal of Chemical Physics **72**, 4350 (1980).

[15] C. Yeung and B. A. Friedman, Europhysics Letters (EPL) **73**, 621 (2006).

[16] G. Wilemski and M. Fixman, The Journal of Chemical Physics **60**, 878 (1974).

[17] P. Debnath and B. J. Cherayil, The Journal of Chemical Physics **120**, 2482 (2004).

[18] D. Panja and G. T. Barkema, The Journal of Chemical Physics **131**, 154903 (2009).

[19] N. M. Toan, G. Morrison, C. Hyeon, and D. Thirumalai, The Journal of Physical Chemistry B **112**, 6094 (2008).

[20] D. Panja, Journal of Statistical Mechanics: Theory and Experiment **2010**, L02001 (2010).

[21] C. Maes and S. R. Thomas, Physical Review E **87** (2013), 10.1103/PhysRevE.87.022145.

[22] H. Vandebroek and C. Vanderzande, Journal of Statistical Physics **167**, 14 (2017).

[23] P. Debnath, W. Min, X. S. Xie, and B. J. Cherayil, The Journal of Chemical Physics **123**, 204903 (2005).

[24] J. Gowdy, M. Batchelor, I. Neelov, and E. Paci, The Journal of Physical Chemistry B **121**, 9518 (2017).

[25] M. Volk, Y. Kholodenko, H. S. M. Lu, E. A. Gooding, W. F. DeGrado, and R. M. Hochstrasser, The Journal of Physical Chemistry B **101**, 8607 (1997).

[26] W. Min, G. Luo, B. J. Cherayil, S. C. Kou, and X. S. Xie, Physical Review Letters **94** (2005), 10.1103/PhysRevLett.94.198302.

[27] M. J. Abraham, T. Murtola, R. Schulz, S. Páll, J. C. Smith, B. Hess, and E. Lindahl, SoftwareX **1-2**, 19 (2015).

[28] C. Oostenbrink, A. Villa, A. E. Mark, and W. F. Van Gunsteren, Journal of Computational Chemistry **25**, 1656 (2004).

[29] J. Kappler, F. Noe, and R. R. Netz, .

[30] B. J. Berne and G. D. Harp, in *Advances in Chemical Physics*, Vol. 17 (John Wiley & Sons, Inc., Hoboken, NJ, USA, 1970) pp. 63–227, dOI: 10.1002/9780470143636.ch3.

[31] J. O. Daldrop, J. Kappler, F. N. Brünig, and R. R. Netz, submitted (2018).

[32] R. Zwanzig, Physical Review **124**, 983 (1961).

[33] H. Mori, Progress of Theoretical Physics **33**, 423 (1965).

[34] M. Doi and S. F. Edwards, *The theory of polymer dynamics*, International series of monographs on physics No. 73 (Clarendon Press, Oxford, 2007) oCLC: 845169495.

[35] A. N. Rissanou, S. H. Anastasiadis, and I. A. Bitsanis, Journal of Polymer Science Part B: Polymer Physics **44**, 3651 (2006).

[36] K. Kremer and K. Binder, The Journal of Chemical Physics **81**, 6381 (1984).

[37] G. S. Grest and K. Kremer, Physical Review A **33**, 3628 (1986).

[38] J. C. F. Schulz, L. Schmidt, R. B. Best, J. Dzubiella, and R. R. Netz, Journal of the American Chemical Society **134**, 6273 (2012).

[39] R. Morgado, F. A. Oliveira, G. G. Batrouni, and A. Hansen, Physical Review Letters **89** (2002), 10.1103/PhysRevLett.89.100601.

[40] D. Ceperley, M. H. Kalos, and J. L. Lebowitz, Physical Review Letters **41**, 313 (1978).

[41] P. G. De Gennes, Macromolecules **9**, 594 (1976).

[42] S. C. Kou and X. S. Xie, Physical Review Letters **93** (2004), 10.1103/PhysRevLett.93.180603.